

# Anisotropic Thermal Diffusivity and Conductivity of La-Doped Strontium Niobate $\text{Sr}_2\text{Nb}_2\text{O}_7$

Taylor D. Sparks

Materials Department, College of Engineering, University of California, Santa Barbara, California 93106-5050

Paul A. Fuierer

Department of Materials and Metallurgical Engineering, New Mexico Institute of Mining and Technology, Socorro, New Mexico 87801

David R. Clarke<sup>†</sup>

School of Engineering and Applied Sciences, Harvard University, Cambridge, Massachusetts 02138

**The thermal diffusivity of the La-doped layered perovskite  $\text{Sr}_2\text{Nb}_2\text{O}_7$  parallel and perpendicular to the perovskite layers is reported from room temperature up to 1000°C. The anisotropy persists through an incommensurate-normal ferroelectric phase transformation at 215°C and up to 1000°C, the maximum temperature of our measurements. The thermal conductivity perpendicular to the perovskite layers, derived from the diffusivity in the same direction, calculated using the density and measured heat capacity, has a constant value of  $1.05 \pm 0.05$  W/mK up to 1000°C. Possible explanations for the low thermal conductivity and anisotropy are described.**

## I. Introduction

Many oxides are crystallographically anisotropic as well as electrically insulating. As such, it might be expected that they will have anisotropic thermal transport properties. Furthermore, many of the anisotropic oxides are natural superlattice structures, consisting of alternating layers or blocks within the unit cell. These include the layered perovskites<sup>1</sup> such as the Aurivillius,<sup>2</sup> Dion-Jacobsen,<sup>3–5</sup> and Ruddlesden-Popper phases.<sup>6,7</sup> Recently, there has been interest in making synthetic superlattices to achieve low thermal conductivity by introducing a high density of interfaces. By this method, very low conductivities have been achieved at low temperatures in  $\text{W}/\text{Al}_2\text{O}_3$  superlattices.<sup>8</sup> For low temperature heat spreading and thermoelectric applications, these synthetic superlattices offer a new approach to heat management. However, they are intrinsically unstable to morphological instability. In contrast, the layered oxides can be expected to be stable to very high temperatures, and hence have high-temperature applications in both heat spreading and as thermal barrier materials.

In a recent work, we have shown that at least two perovskite-based layered oxides exhibit low thermal conductivity. The Aurivillius phase  $\text{Bi}_4\text{Ti}_3\text{O}_{12}$ <sup>9</sup> exhibits anisotropic thermal properties and very low thermal conductivity perpendicular to the layers up to 1000°C. The Ruddlesden-Popper rare-earth strontium aluminates  $\text{RE}_2\text{SrAl}_2\text{O}_7$  (RE = La, Nd, Sm, Eu, Gd, Dy) also have low thermal conductivity.<sup>10</sup> The common features of

both these compounds apart from their crystallographic anisotropy include having large, complex unit cells, a large average atomic volume, and possible structural, bonding and mass disorder, which are all requirements for low thermal conductivity.<sup>11</sup>

Another compound that fits many of these requirements is the layered perovskite  $\text{Sr}_2\text{Nb}_2\text{O}_7$ . The crystal structure of  $\text{Sr}_2\text{Nb}_2\text{O}_7$ , shown in Fig. 1, is a derivative of the perovskite structure, except that the perovskite slabs consisting of vertex-sharing  $\text{NbO}_6$  octahedra are separated by additional O atoms.<sup>12–15</sup> The perovskite layers are offset by a shear of  $a/2$  with respect to one another. The  $\text{Sr}_2\text{Nb}_2\text{O}_7$  compound is a part of a homologous series having a chemical composition  $\text{Sr}_n\text{Nb}_n\text{O}_{3n+2}$ ,<sup>16</sup> where  $n$  denotes the number of  $\text{NbO}_6$  octahedra comprising the slab thickness. Only  $n = 4$  and  $n = 5$  members of the series have been observed so far.<sup>16,17</sup> Because of the layered structure, the thermal properties should be nearly uniaxial along the  $b$ -axis defined to be perpendicular to the layers. Cooling from above the Curie temperature, 1342°C,<sup>18</sup>  $\text{Sr}_2\text{Nb}_2\text{O}_7$  undergoes a ferroelectric phase transition from space group  $Cmcm$  to  $Cmc2_1$ , which is commonly referred to as the normal phase, and on further cooling at 215°C the compound transitions to an incommensurate (IC) phase with space group  $Cmc2_1$ .<sup>19,20</sup>

Single crystals are normally used to determine the principal coefficients of the thermal conductivity tensor and its anisotropy. However, in the absence of large single crystals of  $\text{Sr}_2\text{Nb}_2\text{O}_7$ , an alternative approach based on the symmetry considerations of the thermal conductivity tensor is used in this work by combining measurements of randomly oriented polycrystalline samples and highly-textured samples.

Also, as  $\text{Sr}_2\text{Nb}_2\text{O}_7$  is inherently  $p$ -type, the electronic contribution to thermal conductivity might mask the true nature anisotropy of the thermal conductivity. For this reason, the material measured was doped with a small amount (0.5 mol%) of  $\text{La}^{3+}$  cations substituting for  $\text{Sr}^{2+}$  cations in the unit cell.

## II. Experimental Procedure

### (1) Sample Preparation

Different techniques were used to create the randomly oriented polycrystalline samples and the crystallographically textured samples. The former samples were prepared by conventional sintering and the latter were prepared by hot forging. Sintered samples were prepared by the coprecipitation method described by Brahmaoutou *et al.*<sup>22</sup> Starting materials were  $\text{NbC}_2\text{O}_4$  (Alfa Aesar, purity  $\geq 99.99\%$ ),  $\text{La}_2\text{O}_3$  (Alfa Aesar, Ward Hill, MA; purity  $\geq 99.99\%$ ), and  $\text{Sr}_2\text{NO}_3$  (Sigma Aldrich, St. Louis, MO; purity  $\geq 99.99\%$ ). Stoichiometric quantities

D. J. Green—contributing editor

Manuscript No. 26349. Received June 10, 2009; approved November 11, 2009.

This work was supported under the auspices of a National Science Foundation's Materials World Network grant DMR-0710523 on "Discovery of Low Thermal Conductivity Materials" through the University of California, Santa Barbara.

<sup>†</sup>Author to whom correspondence should be addressed. e-mail: clarke@seas.harvard.edu

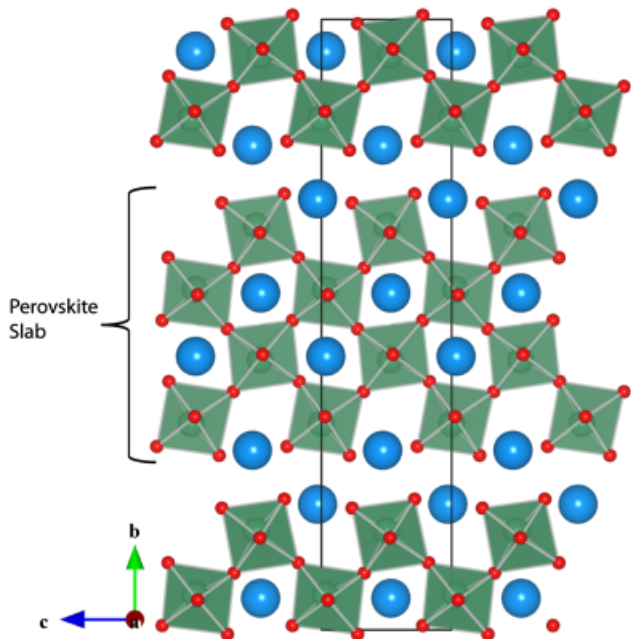


**Fig. 1.** The orthorhombic crystal structure of the  $n=4$  member of  $\text{Sr}_n\text{Nb}_n\text{O}_{3n+2}$  series viewed along the  $a$ -axis. The large spheres are Sr atoms and the octahedral with small sphere vertices are  $\text{NbO}_6$  octahedra. Layers of perovskite-like slabs are separated by additional planes of O atoms. The perovskite slabs are displaced by  $a/2$  with respect to one another. The boxed area represents one unit cell. Image produced using VESTA software.<sup>21</sup>

of  $\text{NbC}_2\text{O}_4$  dissolved in excess oxalic acid,  $\text{La}_2\text{O}_3$  dissolved in excess nitric acid, and  $\text{Sr}_2\text{NO}_3$  dissolved in deionized water were mixed. The resultant solution was coprecipitated by adding it drop by drop to excess NaOH solution maintained at a constant pH of 12 with vigorous stirring. The gel-like precipitants were filtered using a centrifuge, washed twice in deionized water, and then twice in ethanol. The washed precipitates were dried overnight at  $110^\circ\text{C}$  and calcined at  $1000^\circ\text{C}$  for 2 h. The calcined powders were then sieved in a 325 mesh, pressed into 3/4-in. diameter pellets at 200 Mpa, and sintered at  $1400^\circ\text{C}$  for 2 h. The textured samples were prepared by the hot forging method described by Fuierer and Newnham.<sup>23</sup> Starting materials were SrO (Sigma Aldrich, purity  $\geq 99.99\%$ ),  $\text{La}_2\text{O}_3$  (Alfa Aesar, purity  $\geq 99.99\%$ ), and  $\text{Nb}_2\text{O}_5$  (Alfa Aesar, purity  $\geq 99.99\%$ ). The oxide powders were precalcined to  $1000^\circ\text{C}$  for 2 h to remove hydroxide and adsorbed carbon dioxide and water. Powders were weighed and stoichiometric quantities were mixed together and ball milled in ethanol overnight with zirconia media. The mixture was dried and then calcined at  $900^\circ\text{C}$  for 2 h. The powders were sieved in a 325-mesh, pelletized, and then hot forged.<sup>23</sup>

## (2) Characterization

Phase identification and analysis were performed by X-ray diffraction (XRD) using an X-ray diffractometer (Philips X-PERT Pro; Philips, Almelo, the Netherlands) with nickel-filtered  $\text{CuK}\alpha$  radiation. The density ( $\rho$ ) of the samples was measured by the Archimedes method, with deionized water as the immersion medium. The heat capacity ( $C_p$ ) was measured on 1-mm diameter dense pellets using a differential scanning calorimeter (Netzsch, Pegasus 404C, Selb, Bavaria, Germany) in an Argon gas atmosphere from  $35^\circ$  to  $1100^\circ\text{C}$ . The values were determined according to the ASTM standard E1269-95 and the data were collected on heating.

The thermal diffusivity ( $\alpha$ ) was measured using an Anter Flashline 3000 thermal flash system (Pittsburgh, PA) with a high-speed xenon flash lamp. The samples for the thermal diffusivity measurements were machined to be coplanar with a

thickness of approximately 1 mm and a diameter of 12.5 mm. Before the measurements, both sides of each sample were coated with thin layers of Ti and Pt using electron beam physical vapor deposition to minimize the possibility of radiative transport through the translucent samples and any associated with pinholes. The Ti adhesion layer was approximately 10 nm thick while the Pt layer was about 750 nm. The samples were then spray coated with colloidal graphite on both sides to ensure full absorption and maximum optical absorption and emissivity. Thermal diffusivity was measured in an Argon gas atmosphere from  $35^\circ$  to  $1000^\circ\text{C}$  at intervals of  $100^\circ\text{C}$  with a comparison measurement at  $100^\circ\text{C}$  when cooling down to ensure reproducibility of the measurements and to identify if the coatings remained intact. The thermal diffusivity values were determined using the Clarke and Taylor<sup>24</sup> model, which corrects for radiative losses from the sample during the test. Correction of the high-temperature diffusivity measurements for radiative heat transfer through the samples was performed using a numerical method.<sup>25</sup>

## III. Results

### (1) XRD

The X-ray results, shown in Fig. 2, indicate that both the sintered and hot-forged samples were single phase. All the peaks correspond to the orthorhombic phase.<sup>26</sup> The hot-forged sample exhibited very strong  $(0k0)$  peaks. The other peaks found in random samples and listed in the JCPDS file here absent. This indicates that the hot-forged samples were strongly textured along the crystallographic  $b$ -axis. The degree of orientation was quantified by calculating the Lotgering factor  $f$  from the X-ray peak intensities<sup>27</sup> over the range of  $10^\circ$ – $90^\circ$ . For the hot-forged samples, the maximum out-of-plane grain orientation was found to be  $>95\%$  after polishing away the surface in preparation for the diffusivity measurements.

### (2) Density

The densities of the samples were 5197 and  $5267\text{ kg/m}^3$  for the textured and polycrystalline samples, respectively. The theoretical density of  $\text{La}_{0.005}\text{Sr}_{1.995}\text{Nb}_2\text{O}_7$  assuming an orthorhombic unit cell with lattice parameters  $a = 0.3933\text{ nm}$ ,  $b = 2.6726\text{ nm}$ , and  $c = 0.5683\text{ nm}$  is  $5316\text{ kg/m}^3$ . Therefore, both sets of samples were determined to be greater than 97% dense.

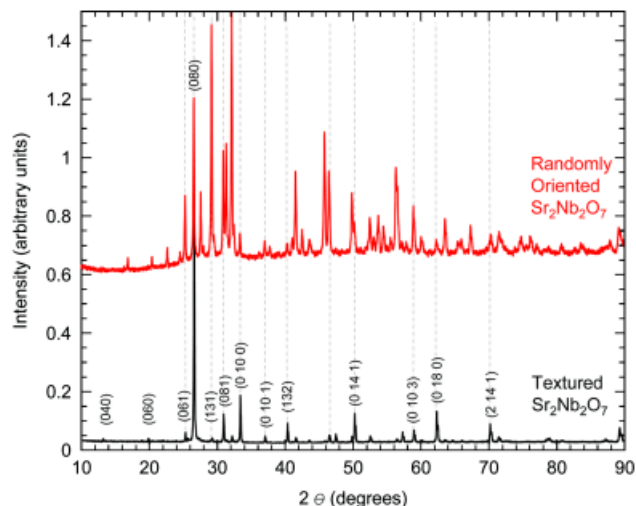


**Fig. 2** Normalized X-ray diffraction patterns from randomly oriented (above) and hot-forged, textured (below) samples of  $\text{Sr}_2\text{Nb}_2\text{O}_7$ . Diffracted intensity from peaks corresponding to  $(0k0)$  dominates in the textured sample whereas the randomly oriented polycrystalline sample matches the expected peak pattern for  $\text{Sr}_2\text{Nb}_2\text{O}_7$  orthorhombic unit cell.

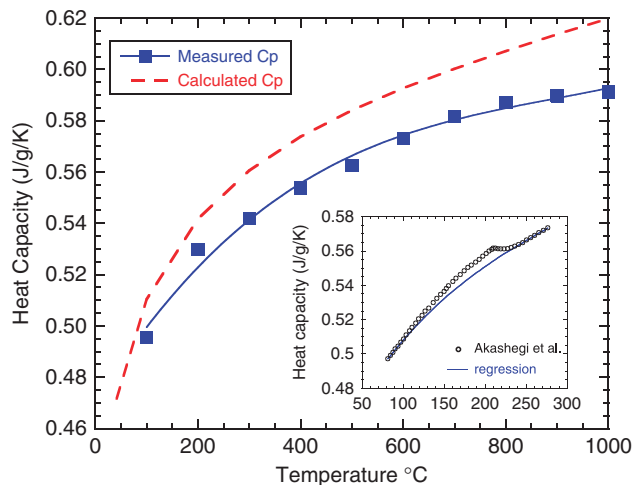


**Fig. 3** Heat capacity of powder from a crushed sample of the textured  $\text{Sr}_2\text{Nb}_2\text{O}_7$ . Measurement are compared with calculations according to the Neumann–Kopp rule (dashed line) and shown to be within 4.2%. The solid line is a guide for the eye. The second-order phase transition is shown in the inset along with the extrapolated baseline.

### (3) Heat Capacity

The temperature dependence of the heat capacity is shown in Fig. 3. The heat capacity increases monotonically with temperature except close to the second-order phase transition<sup>28</sup> of the normal phase at  $\approx 215^\circ\text{C}$  indicated by the small exothermic peak. The heat capacity data were compared by also calculating the heat capacity according to the Neumann–Kopp rule from the chemical compositions and the literature data of its constituent oxides.<sup>29</sup> The calculated values for heat capacity were within  $\pm 4.2\%$  of the measured values.

### (4) Thermal Diffusivity

The thermal diffusivity measurements are shown in Fig. 4. There are two regimes discernable, one below and one above the temperature of the phase transition from the normal phase to the IC phase. The lower temperature regime is more strongly temperature dependent with a slope ranging from  $-1.8 \times 10^{-6}$  to  $-4.8 \times 10^{-6} \text{ cm}^2/\text{s K}$ . Remarkably, the diffusivity of the

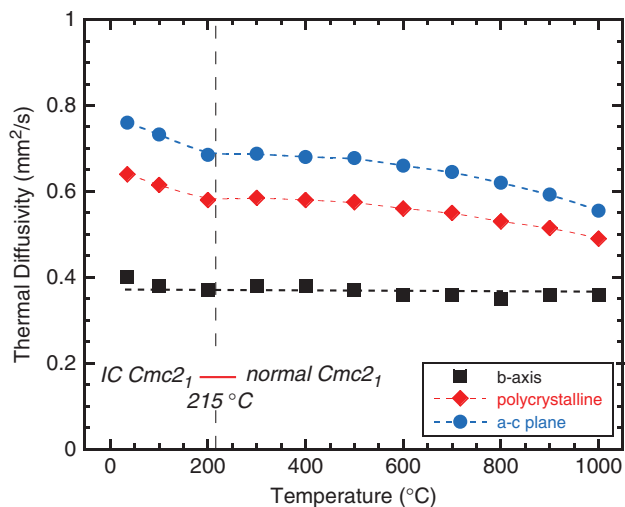


**Fig. 4** Thermal diffusivity as a function of temperature along the  $b$ -axis in a highly textured ceramic and of the randomly oriented polycrystalline material. The thermal conductivity along the layered planes ( $a$ - $c$  plane), determined from the other diffusivities, is also shown. The dashed lines are guides to the eye except for those through the  $b$ -axis data, which are a least square fit.

textured sample was constant over the entire temperature range whereas that of the randomly oriented polycrystalline sample decreased slightly with temperature above the transition temperature.

## IV. Discussion

The diffusivity measurements in Fig. 4 clearly show that the diffusivity perpendicular to the perovskite layers is substantially smaller than that of the randomly oriented polycrystalline material. Furthermore, the diffusivity is unusually small and temperature independent up to the maximum temperature we could measure. Although samples textured with the perovskite layers parallel to the heat propagation direction are not available, the well-defined crystallography of the two polycrystalline materials enables the diffusivity parallel to the perovskite layers to be calculated using tensorial analysis<sup>30</sup> from the results of the hot-forged and sintered materials as follows.

For an orthorhombic structure, the thermal diffusivity tensor,  $\alpha_{ij}$ , a second-rank tensor, can be expressed in terms of the diffusivity along the principal crystallographic axes as

$$\alpha_{ij} = \begin{pmatrix} \alpha_{aa} & 0 & 0 \\ 0 & \alpha_{bb} & 0 \\ 0 & 0 & \alpha_{cc} \end{pmatrix} \quad (1)$$

where the subscripts refer to the crystallographic directions in the unit cell. Although the unit cell of the  $\text{Sr}_2\text{Nb}_2\text{O}_7$  structure is strictly orthorhombic, the lattice parameters and sound velocities along the  $a$ - and  $c$ -axes are very similar. The longitudinal sound velocities ( $v$ ) along the  $a$ -,  $b$ -, and  $c$ -axes have been measured by Brillouin scattering and are reported to be  $4438 \pm 25$ ,  $5192 \pm 12$ , and  $4458 \pm 19$  m/s, respectively.<sup>28</sup> (The shear velocities, as far as we can determine, have not been measured.) The  $a$ - and  $c$ -lattice parameters are reported to be 0.3933 and 0.5683 nm, respectively, whereas the  $b$ -lattice parameter is 2.6726 nm. Consequently, we can assume that the thermal properties along the  $a$ - and  $c$ -axes are also likely to be similar. This assumption allows the diffusivity tensor to be represented by a uniaxial tetragonal tensor

$$\alpha_{ij} = \begin{pmatrix} \alpha_{aa} & 0 & 0 \\ 0 & \alpha_{bb} & 0 \\ 0 & 0 & \alpha_{cc} \end{pmatrix} = \begin{pmatrix} \alpha_{aa} & 0 & 0 \\ 0 & \alpha_{bb} & 0 \\ 0 & 0 & \alpha_{cc} \end{pmatrix} \quad (2)$$

For randomly oriented polycrystalline material, the thermal diffusivity,  $\alpha_p$ , can be expressed in terms of the trace of the tensor (appendix in reference<sup>31</sup>), namely as

$$\alpha_p = 1/3(2\alpha_{aa} + \alpha_{bb}) \quad (3)$$

Rearranging Eq. (3) and assuming 100% texturing, the thermal diffusivity within the  $a$ - $c$  plane,  $\alpha_{aa}$ , can be calculated from the measured diffusivities of the polycrystalline material and the textured hot-forged samples

$$\alpha_{aa} = 1/2(3\alpha_p + \alpha_{bb}) \quad (4)$$

The calculated values for the diffusivity parallel to the perovskite planes are shown in the graph of Fig. 4 by the circular symbols. Comparison with the other data indicates that the diffusivity is significantly higher, by almost a factor of two, parallel to the planes than perpendicular to the perovskite planes.

An interesting feature of the diffusivity measurements (Fig. 4) is that the anisotropy is much larger than the anisotropy in either the lattice parameters or the sound velocities. The former is 50% larger in the  $b$ -direction than in the other directions

whereas the sound velocity is only 16% larger. We will return to this point later in Section IV.

The thermal conductivity is also a second-rank tensor and can be computed from the diffusivity using the relationship

$$k_{ij} = \rho C_p \alpha_{ij} \quad (5)$$

Using this relationship as a definition, the conductivities parallel and perpendicular to the perovskite layers can be computed and are shown in Fig. 5. The density is assumed to decrease with increasing temperature in accord with an average linear coefficient of thermal expansion of  $10^{-5}$ .

The temperature dependence of the thermal conductivity of the La-doped  $\text{Sr}_2\text{Nb}_2\text{O}_7$  shown in Fig. 5, is notable in three major respects. Firstly, the thermal conductivity, especially perpendicular to the perovskite layers, is very low and is temperature independent in contrast to that usually found for defect-free oxides.<sup>32</sup> The temperature range of the measurements also spans the Debye temperature,  $\Theta_D$  (340°C) calculated using the relationship

$$\Theta_D = \frac{\hbar}{k_B} \left( \frac{6\pi^2}{\bar{\Omega}} \right)^{1/3} v_m$$

where  $\bar{\Omega}$  is the mean atomic volume,  $v_m$  is the average phonon velocity,  $\hbar$  is Planck's constant, and  $k_B$  is Boltzmann's constant. Secondly, the thermal conductivity does not change, within experimental uncertainty, in crossing the phase transition at 215°C. Thirdly, the thermal diffusivity and conductivity are strongly anisotropic over the entire temperature range measured, up to 1000°C. These features will be discussed in turn in the following.

Oxides that typically exhibit little or no temperature dependence are either amorphous, such as silica, or contain very high concentrations of point defects. The latter is exemplified by yttria-stabilized zirconia, which typically contains several percent of oxygen vacancies. In both classes of material, the thermal conductivity is limited as the mean free path approaches atomic dimensions even at temperatures as low as room temperature. In the case of amorphous materials, the minimum phonon mean free path is limited by the size of the structural unit making up the amorphous structure.<sup>33</sup> In the concentrated defect-scattering case, such as yttria-stabilized zirconia, the conductivity is limited as the phonon mean free path approaches the average defect spacing. The temperature dependence of the thermal conductivity

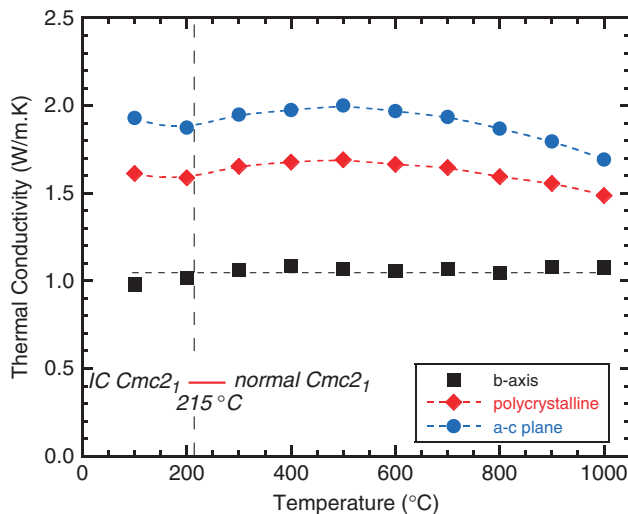


**Fig. 5** Thermal conductivity as a function of temperature along the *b*-axis of the highly textured materials and of the randomly oriented polycrystalline material. The calculated thermal conductivity in the plane of the perovskite layers (the *a-c* plane) is also shown.

ity is then weakened and in the extreme cases of small defect, spacing becomes almost independent of temperature, approaching the minimum thermal conductivity value,  $k_{\min}$ . The minimum thermal conductivity, which we take as the minimum for the randomly oriented polycrystalline material,  $k_{\text{pm}}$ , can be estimated from the high-temperature limit of the Debye equation,<sup>34</sup>

$$k_p \rightarrow k_{\text{pm}} = \frac{C_V v_m \Lambda}{3} \quad (7)$$

where  $C_V$  is the specific heat at constant volume and  $\Lambda$  is the phonon mean free path. At high temperatures, the specific heat per atom  $C_V$  approaches a value of  $3k_B T$ , according to the Dulong–Petit equation,<sup>34</sup> and hence the minimum thermal conductivity becomes

$$k_{\text{pm}} = \frac{k_B v_m \Lambda}{\bar{\Omega}} \quad (8)$$

Inverting this equation, the phonon mean free path can be calculated from the conductivity of the randomly oriented material. In the absence of information about the shear velocities, the phonon mean free path,  $\Lambda$ , is estimated to be 0.301 nm using values for the average velocity of sound  $v_m$  of  $\sim 4900$  m/s<sup>28</sup> and the average atomic volume ( $\bar{\Omega}_a$ ) of  $\text{Sr}_2\text{Nb}_2\text{O}_7$  of  $0.01370$  nm<sup>3</sup>. This value is almost identical to the value of the mean inter-atomic spacing (0.296 nm) obtained by assuming that the mean atomic volume is spherical. This result is consistent with the temperature independence of the thermal conductivity, which suggests that the phonon mean free path is comparable with the inter-atomic spacings in the structure. If the conductivity perpendicular to the perovskite layers,  $\sim 1.0$  W/mK, is used in the estimate, the calculated phonon mean free path is 0.2 nm, which is similar to the thickness of the individual perovskite layers (0.27 nm) and the separation between the perovskite blocks (0.236 nm). Thus, it can be concluded that it is reasonable that the effective phonon mean free path is of the same length scale as the inter-atomic spacings.

An alternative explanation for the temperature independence of the conductivity is that the observed conductivity is not the minimum conductivity determined by the mean inter-atomic spacing but rather by scattering from closely spaced defects. In this explanation, the defects are responsible for decreasing the thermal conductivity from the temperature dependence of the perfect crystal to the value given by  $k_{\text{pm}}$ . Three types of defects in La-doped  $\text{Sr}_2\text{Nb}_2\text{O}_7$  can be identified: the  $\text{La}^{3+}$  dopant ions themselves, the associated cation vacancies required to maintain overall charge neutrality (one vacancy for each two  $\text{La}^{3+}$  ions) and anti-site cation defects in which an  $\text{Sr}^{2+}$  ion is on an  $\text{Nb}^{5+}$  ion site, and vice-versa. The average spacing between dopant ions, randomly distributed within a volume of material, varies with concentration,  $c$ , as  $c^{-1/3}$ . The  $\text{La}^{3+}$  dopant concentration in the material we have studied is 0.5 mol%. Assuming that they are randomly distributed, the average spacing between  $\text{La}^{3+}$  ions is 2.47 nm. The average spacing between the cation vacancies is 3.07 nm. Both these defect spacings are an order of magnitude larger than the inter-atomic distances, and hence it is unlikely that this alone could account for enough ionic disorder or structural defects to lower the phonon mean free path so significantly. For comparison, the average distance between the  $\text{La}^{3+}$  ions is substantially larger than the oxygen vacancy spacing, which is  $\sim 0.76$  nm in yttria-stabilized zirconia.<sup>35</sup> The phonon scattering from the  $\text{La}^{3+}$  ions and the cation vacancies, however, is expected to be different as their masses are different. According to Klemens,<sup>36,37</sup> the phonon scattering from defects having different masses depends on the parameter,  $\Gamma$ , given by

$$\Gamma = \sum_i f_i \left( 1 - \frac{M_i}{M} \right)^2 \quad (9)$$

where  $f_i$  is the fraction of defects having a mass  $M_i$  and  $M$  is the mass of the atoms in the lattice. For a material containing two defects of different masses, in this material an  $\text{La}^{3+}$  ion (138.9 amu) on an Sr site (87.6 amu) and a cation vacancy on a Sr site, this scattering can be generalized as

$$\Gamma = f_{\text{La}} \left( \frac{M - M_{\text{La}}}{M} \right)^2 + f_{\text{vac}} \left( \frac{M - M_{\text{vac}}}{M} \right)^2 \quad (10)$$

An interesting feature of this equation for the scattering factor is that the mass difference associated with the cation vacancies is larger than the mass difference associated with the  $\text{La}^{3+}$  ion substitution. As a result, the two terms contributing to the overall mass difference scattering are almost the same after taking into account the difference in the concentration of the two defects. The third possible contribution to phonon scattering is site disorder of the  $\text{Sr}^{2+}$  and  $\text{Nb}^{5+}$  ions in the lattice. However, it is unlikely that appreciable site disorder is possible in the crystal structure of the niobate given the different ionic sizes and site coordination preferences of the  $\text{Sr}^{2+}$  and  $\text{Nb}^{5+}$  ions. Furthermore, the atomic masses of Sr (87.6 amu) is similar to that of Nb (92.9 amu) and hence even if there were any appreciable site disorder, the effect on phonon scattering is likely to be small as seen from Eq. (9), assuming that there are no significant differences in the bond strength.

Although it can be concluded that defect scattering from the  $\text{La}^{3+}$  ions and cation vacancies can be appreciable, their spacing is rather large compared with the inter-atomic spacing for the composition investigated and thus is unlikely to account for the very low thermal conductivities we observed. However, we should point out that a feature of defect scattering is that it is temperature independent as are our data.<sup>37</sup>

The insensitivity of the thermal conductivity to the phase transition as the material transforms from the IC to the normal ferroelectric orthorhombic phase may appear to be surprising. This is especially so as there are large IC modulations of the structure below the transition temperature.<sup>38</sup> These IC modulations result in rotational oscillations of the  $\text{NbO}_6$  octahedra and large time-dependent displacements of the Sr ions<sup>38</sup> and are presumably responsible in part for the marked increase in heat capacity as the transition temperature (inset in Fig. 3) is approached from lower temperatures. However, there appear to be two compensating effects associated with the differing temperature dependence of the diffusivity and the specific heat. As indicated by the data in Fig. 4, there is a slight change in temperature dependence of the diffusivity as the material transforms from the IC to the normal orthorhombic phase at 215°C, although the change is small. This is also in the temperature range over which the specific heat varies strongly with temperature but with a monotonically decreasing slope and hence the effect on the calculated conductivity is suppressed. In addition, the sound velocity decreases with increasing temperature over the same temperature range further suppressing any change in thermal conductivity in crossing the phase transformation. It should also be noted that a similar insensitivity to a structural rearrangement at a ferroelectric transition has been reported for the Aurivillius structure compound,  $\text{Bi}_4\text{Ti}_3\text{O}_{12}$ , which is also a layered ferroelectric oxide and has a ferroelectric transition temperature of 675°C.<sup>9</sup>

Lastly, as shown in Fig. 5, there is a relatively large anisotropy in thermal conductivity that remains up to at least 1000°C. No quantitative explanation exists as far as we are aware. However, one possible explanation would be if there is a significant difference in anharmonicity parallel and perpendicular to the perovskite layers. In support of this possibility is that the blocks of four perovskite layers are separated by an intermediary layer of oxygen ions with strontium ions at the interfaces between the perovskite blocks whereas the bonding in the perovskite layers is more isotropic. Brillouin scattering indicates that there is some elastic anisotropy with  $c_{11}$ ,  $c_{33}$ , and  $c_{22}$  being 10.19, 10.27, and

13.9 ( $\times 10^{10}$  N/m<sup>2</sup>)<sup>28</sup> but this is, in effect, an elastic modulus averaged over distances larger than the unit cell whereas the phonon wavelengths contributing to the thermal conductivity are commensurate with the inter-atomic spacings. Thus, one possible explanation is that the intermediary layer of oxygen–strontium bonding between the perovskite blocks provides the anharmonicity essential for lowering the conductivity perpendicular to the blocks. Diffraction studies using a synchrotron<sup>38</sup> reveal that these Sr ions are displaced from the ideal perovskite-like sites and that there are IC modulations associated with these ions. Furthermore, they have a complicated 10-fold coordination rather than the usual 12-fold coordination in the ideal perovskite. These would also be consistent with the observation that the thermal anisotropy persists to high temperatures. A more direct measure of anharmonicity, such as a difference in thermal expansion of the unit cell perpendicular and parallel to the perovskite layers, would be desirable. For instance, a pronounced difference in thermal expansion has been computed for  $\text{Bi}_2\text{Te}_3$ , another block-like layered structure, which exhibits thermal conductivity anisotropy parallel and perpendicular to its layers.<sup>39</sup> Lastly, it has been noted that crystals can be easily cleaved parallel to the perovskite layers and this property has been used in aligning crystals for XRD studies.

It is also tempting to suggest that the anisotropy is a consequence of phonon scattering by the natural superlattice of repeating  $(\text{SrO}_2)^{2-}$  and  $(\text{Sr}_3\text{Nb}_5\text{O}_{12})^{2+}$  blocks of perovskite that comprise the layered structure of the strontium niobate. We note that there is a substantial mass difference between the blocks in the crystal structure which would result in significant phonon velocity mismatch. In the normal phase, the density of the  $(\text{SrO}_2)^{2-}$  block is 3.733 g/cm<sup>3</sup> and the thickness is 0.236 nm whereas the  $(\text{Sr}_3\text{Nb}_5\text{O}_{12})^{2+}$  block of four perovskite layers has a density of 5.527 g/cm<sup>3</sup> and a thickness of 1.102 nm. The ratio of the density of the different blocks is rather large (1.48:1) possibly resulting in significant acoustic mismatch for phonon scattering.

## V. Summary

The thermal properties of highly textured and polycrystalline samples of 0.5 mol% La-doped  $\text{Sr}_2\text{Nb}_2\text{O}_7$  have been measured from just above room temperature (35°C) to 1000°C. The thermal conductivity was found to be very low ( $\sim 1$  W/mK), temperature independent, and strongly anisotropic parallel and perpendicular to the layered structure up to 1000°C. The phase transition between the room temperature IC orthorhombic phase and the normal orthorhombic phase above 215°C has a negligible effect on thermal conductivity. As with our previous studies on related layered perovskites, it is tempting to attribute the thermal anisotropy and low conductivity to the density difference between the  $(\text{SrO}_2)^{2-}$  block and the pseudo-perovskite  $(\text{Sr}_3\text{Nb}_5\text{O}_{12})^{2+}$  block in the natural superlattice structure of the strontium niobate.

## References

- <sup>1</sup>R. Mitchell, *Perovskites Modern and Ancient*. Almaz, Thunder Bay, Canada, 2002.
- <sup>2</sup>B. Aurivillius, "Mixed Bismuth Oxides with Layer Lattices: II. Structure of  $\text{Bi}_4\text{Ti}_3\text{O}_{12}$ ," *Arkiv for Kemi*, **1** [58] 499–512 (1949).
- <sup>3</sup>M. Dion, M. Ganne, and M. Tournoux, "Probing Octahedral Tilting in Dion-Jacobson Layered Perovskites with Neutron Powder Diffraction and Raman Spectroscopy," *Mater. Res. Bull.*, **16**, 1429–35 (1981).
- <sup>4</sup>M. Dion, M. Ganne, M. Tournoux, and J. Ravez, *Rev. Chim. Minerale*, **21**, 92–103 (1984).
- <sup>5</sup>M. Dion, M. Ganne, and M. Tournoux, *Rev. Chim. Miner.*, **23**, 61–9 (1986).
- <sup>6</sup>S. N. Ruddlesden and P. Popper, "New Compounds of the  $\text{K}_2\text{NiF}_4$  Type," *Acta Crystallogr.*, **10** [8] 538–9 (1957).
- <sup>7</sup>S. N. Ruddlesden and P. Popper, "On the Crystal Structure of the Nitrides of Silicon and Germanium," *Acta Crystallogr.*, **11** [7] 465–8 (1958).
- <sup>8</sup>R. M. Costescu, D. G. Cahill, F. H. Fabequette, Z. A. Sechrist, and S. M. George, "Ultra-Low Thermal Conductivity in  $\text{W}/\text{Al}_2\text{O}_3$  Nanolaminates," *Science*, **303** [5660] 989–90 (2004).
- <sup>9</sup>Y. Shen, D. R. Clarke, and P. A. Fuierer, "Anisotropic Thermal Conductivity of the Aurivillius Phase, Bismuth Titanate ( $\text{Bi}_4\text{Ti}_3\text{O}_{12}$ ): A Natural Nanostructured Superlattice," *App. Phys. Lett.*, **93**, 102907, 3pp (2008).

- <sup>10</sup>C. L. Wan, T. D. Sparks, P. Wei, and D. R. Clarke, "Thermal Conductivity of the Rare-Earth Strontium Aluminates," *J. Am. Ceram. Soc.* (2009), in press.
- <sup>11</sup>D. R. Clarke, "Materials Selection Guidelines for Low Thermal Conductivity Thermal Barrier Coatings," *Surf. Coat. Technol.*, **163–164**, 67–74 (2003).
- <sup>12</sup>N. Ishizawa, F. Marumo, T. Kawamura, and M. Kimura, "The Crystal Structure of  $\text{Sr}_2\text{Nb}_2\text{O}_7$ , a Compound with Perovskite-Type Slabs," *Acta Crystallogr. Sec. B*, **31** [7] 1912–15 (1975).
- <sup>13</sup>H. W. Schmalle, T. Williams, A. Reller, F. Lichtenberg, D. Widmer, and J. G. Bednorz, "A Novel Semiconducting Perovskite-Related Phase:  $\text{Sr}_5\text{Nb}_5\text{O}_{17}$ ," *Acta Crystallogr. Sec. C*, **51** [7] 1243–46 (1995).
- <sup>14</sup>S. C. Abrahams, H. W. Schmalle, T. Williams, Williams, A. Reller, F. Lichtenberg, D. Widmer, J. G. Bednorz, R. Spreiter, Ch. Bosshard, and P. Günter, "Centrosymmetric or Noncentrosymmetric? Case Study, Generalization and Structural Redetermination of  $\text{Sr}_3\text{Nb}_3\text{O}_{17}$ ," *Acta Crystallogr.*, **B54**, 399–416 (1998).
- <sup>15</sup>L. Elcoro, J. M. Perez-Mato, and R. L. Withers, "Intergrowth Polytypoids as Modulated Structures: A Superspace Description of the  $\text{Sr}_m(\text{Nb,Ti})_n\text{O}_{3n} + 2$  Compound Series," *Acta Crystallogr. Sec. B*, **57** [4] 471–84 (2001).
- <sup>16</sup>T. Williams, F. Lichtenberg, D. Widmer, J. G. Bednorz, and A. Reller, "Layered Perovskitic Structures in Pure and Doped  $\text{LaTiO}_{3.5-x}$  and  $\text{SrNbO}_{3.5-x}$ ," *J. Solid State Chem.*, **103** [2] 375–86 (1993).
- <sup>17</sup>F. Lichtenberg, A. Herrnberger, K. Wiedenmann, and J. Mannhart, *Prog. Solid State Chem.*, **29**, 1–70 (2001).
- <sup>18</sup>K. Ohi and S. Kojima, "Successive Phase Transitions and their Soft Modes in Ferroelectric  $\text{Sr}_2\text{Nb}_2\text{O}_7$ ," *Jpn. J. Appl. Phys.*, **24** [24–2] 817–19 (1985).
- <sup>19</sup>N. Yamamoto, K. Yagi, G. Honjo, M. Kimura, and T. Kawamura, "New Phases of  $\text{Sr}_2\text{Ta}_2\text{O}_7$  and  $\text{Sr}_2\text{Nb}_2\text{O}_7$  Found by Electron Microscopy and Diffraction," *J. Phys. Soc. Jpn.*, **48**, 185–91 (1980).
- <sup>20</sup>N. Yamamoto, "High-Resolution Electron Microscopy of the Incommensurate Structure in  $\text{Sr}_2\text{Nb}_2\text{O}_7$ ," *Acta Crystallogr. Sec. A*, **38** [6] 780–9 (1982).
- <sup>21</sup>K. Momma and F. Izumi, "VESTA: A Three Dimensional Visualization System for Electronic and Structural Analysis," *J. Appl. Crystallogr.*, **41**, 653–658 (2008).
- <sup>22</sup>B. Brahmarouti, G. L. Messing, and S. Trolier-McKinstry, "Densification and Anisotropic Grain Growth in  $\text{Sr}_2\text{Nb}_2\text{O}_7$ ," *J. Mater. Sci.*, **35** [22] 5673–80 (2000).
- <sup>23</sup>P. A. Fuierer and R. E. Newnham, " $\text{La}_2\text{Ti}_2\text{O}_7$  Ceramics," *J. Am. Ceram. Soc.*, **74** [11] 2876–81 (1991).
- <sup>24</sup>L. I. Clarke and R. Taylor, "Radiation Loss in the Thermal Flash Method for Thermal Diffusivity," *J. Appl. Phys.*, **46** [2] 714–9 (1975).
- <sup>25</sup>L. Chen and D. R. Clarke, "A Numerical Solution Based Parameter Estimation Method for Flash Thermal Diffusivity Measurements," *Comput. Mater. Sci.*, **45**, 342–8 (2009).
- <sup>26</sup>D. R. Clarke and R. Tandon, "Factors Affecting the Fracture-Resistance of Silicon-Nitride Ceramics," *Mater. Sci. Eng. A—Struct. Mater. Prop. Microstruct. Process.*, **195** [1–2] 207–14 (1995).
- <sup>27</sup>F. K. Lotgering, "Topotactical Reactions with Ferrimagnetic Oxides Having Hexagonal Crystal Structures—I," *J. Inorg. Nucl. Chem.*, **9**, 113–23 (1959).
- <sup>28</sup>G. Shabbir and S. Kojima, "Acoustic and Thermal Properties of Strontium Pyroniobate Single Crystals," *J. Phys. D: Appl. Phys.*, **8**, 1036–9 (2003).
- <sup>29</sup>I. Barin, *Thermochemical Data of Pure Substances*. VCH, Weinheim, 1993.
- <sup>30</sup>J. F. Nye, *Physical Properties of Crystals. Their Representation by Tensors and Matrices*. Oxford Science Publications, Oxford, UK, 1985.
- <sup>31</sup>Q. Ma and D. R. Clarke, "Stress Measurement in Single-Crystal and Polycrystalline Ceramics Using their Optical Fluorescence," *J. Am. Ceram. Soc.*, **76** [6] 1433–40 (1993).
- <sup>32</sup>W. D. Kingery, "Thermal Conductivity: XII, Temperature Dependence of Conductivity for Single-Phase Ceramics," *J. Am. Ceram. Soc.*, **38** [7] 251–55 (1955).
- <sup>33</sup>C. Kittel, "Interpretation of the Thermal Conductivity of Glasses," *Phys. Rev.*, **75** [6] 972–4 (1949).
- <sup>34</sup>C. Kittel, *Introduction to Solid State Physics*. Wiley, New York, 1986.
- <sup>35</sup>V. Lughi and D. R. Clarke, "Transformation of Electron-Beam Physical Vapor-Deposited 8 wt% Ytria-Stabilized Zirconia Thermal Barrier Coatings," *J. Am. Ceram. Soc.*, **88** [9] 2552–8 (2005).
- <sup>36</sup>P. G. Klemens, "The Scattering of Low-Frequency Lattice Waves by Static Imperfections," *Proc. Phys. Soc. London Sec. A*, **68** [12] 1113–28 (1955).
- <sup>37</sup>J. Callaway and H. C. von Baeyer, "Effect of Point Imperfections on Lattice Thermal Conductivity," *Phys. Rev.*, **120** [4] 1149–54 (1960).
- <sup>38</sup>P. Daniels, R. Tamazyan, C. A. Kuntscher, M. Dressel, F. Lichtenberg, and S. van Smaalen, "The Incommensurate Modulation of the Structure of  $\text{Sr}_2\text{Nb}_2\text{O}_7$ ," *Acta Crystallogr.*, **B58**, 970–7 (2002).
- <sup>39</sup>B.-L. Huang and M. Kaviani, "Ab-Initio and Molecular Dynamics Predictions for Electron and Phonon Transport in Bismuth Telluride," *Phys. Rev. B*, **77**, 125209, 19pp (2008). □